ADVANCES IN ATMOSPHERIC SCIENCES, VOL. 32, JUNE 2015, 839–854

Precipitation Changes in Wet and Dry Seasons over the 20th Century Simulated by Two Versions of the FGOALS Model

MA Shuangmei[1,2] and ZHOU Tianjun*[1,3]

[1] *State Key Laboratory of Numerical Modeling for Atmospheric Sciences and Geophysical Fluid Dynamics, Institute of Atmospheric Physics, Chinese Academy of Sciences, Beijing* 100029

[2] *University of Chinese Academy of Sciences, Beijing* 100049

[3] *Climate Change Research Center, Chinese Academy of Sciences, Beijing* 100029

(Received 24 June 2014; revised 10 October 2014; accepted 29 October 2014)

ABSTRACT

Seasonal precipitation changes over the globe during the 20th century simulated by two versions of the Flexible Global Ocean–Atmosphere–Land System (FGOALS) model are assessed. The two model versions differ in terms of their AGCM component, but the remaining parts of the system are almost identical. Both models reasonably reproduce the mean-state features of the timings of the wet and dry seasons and related precipitation amounts, with pattern correlation coefficients of 0.65–0.84 with observations. Globally averaged seasonal precipitation changes are analyzed. The results show that wet seasons get wetter and the annual range (precipitation difference between wet and dry seasons) increases during the 20th century in the two models, with positive trends covering most parts of the globe, which is consistent with observations. However, both models show a moistening dry season, which is opposite to observations. Analysis of the globally averaged moisture budget in the historical climate simulations of the two models shows little change in the horizontal moisture advection in both the wet and dry seasons. The globally averaged seasonal precipitation changes are mainly dominated by the changes in evaporation and vertical moisture advection. Evaporation and vertical moisture advection combine to make wet seasons wetter and enhance the annual range. In the dry season, the opposite change of evaporation and vertical moisture advection leads to an insignificant change in precipitation. Vertical moisture advection is the most important term that determines the changes in precipitation, wherein the thermodynamic component is dominant and the dynamic component tends to offset the effect of the thermodynamic component.

Key words: 20th century historical climate simulation, FGOALS-g2, FGOALS-s2, wet season, dry season, precipitation change, water vapor budget diagnosis

Citation: Ma, S. M., and T. J. Zhou, 2015: Precipitation changes in wet and dry seasons over the 20th century simulated by two versions of the FGOALS model. *Adv. Atmos. Sci.*, **32**(6), 839–854, doi: 10.1007/s00376-014-4136-x.

1. Introduction

Precipitation is not only a natural feature of Earth's weather systems, but also has an irreplaceable role in the global hydrological cycle. As the rainfall amount, intensity and frequency vary spatially and temporally, rainfall plays a key role in forming the climate of certain areas. However, some changes in precipitation, e.g. the intensity and frequency increases that have led to severe drought and flooding during the last three decades (Allan and Soden, 2008), may exert adverse effects on agriculture, water resources, human health and infrastructure. Understanding the main characteristics of and reasons for precipitation changes has therefore become a major focus of the climate change research community and is of great concern to society.

Great efforts have been devoted to understanding how the global hydrological cycle, in particular global precipitation, responds to a warming climate (Held and Soden, 2006; Vecchi and Soden, 2007; Wentz et al., 2007; Zhang et al., 2007; Trenberth, 2011; William et al., 2013). Under global warming, the global-mean precipitation simulated by global coupled atmosphere–ocean general circulation models (AOGCMs) tends to increase at a rate of about 1% to 3% K^{-1} (Held and Soden, 2006; Vecchi and Soden, 2007; Andrews et al., 2010). In a warming climate, coupled climate models project globally more heavy precipitation, less moderate precipitation, and more light precipitation (Allan and Soden, 2008; Allan et al., 2010; William et al., 2013). In addition to an increase in global-mean precipitation, coupled AOGCMs suggest that global warming causes a latitudinal redistribution of precipitation, with increasing precipitation at high and deep tropical latitudes, and decreasing precipitation at subtropical latitudes (Held and Soden, 2006; Zhang et

* Corresponding author: ZHOU Tianjun
Email: zhoutj@lasg.iap.ac.cn

al., 2007; Scheff and Frierson, 2012; Noake et al., 2012; Polson et al., 2013). The above-mentioned precipitation changes are evident in observations, but the amplitudes of the changes simulated by coupled climate models are generally smaller than observed (Zhang et al., 2007; Allan et al., 2010; Zhou et al., 2011; Noake et al., 2012).

The main contribution of global-mean precipitation comes from tropical convective precipitation. The pattern of tropical precipitation change is dominated by two mechanisms: "wet-get-wetter" (Chou and Neelin, 2004) and "warmer-get-wetter" (Xie et al., 2010). The wet-get-wetter mechanism argues that precipitation increases in the core of major tropical rainbands (Allan et al., 2010; Zhou et al., 2011). This pattern is generally explained by the increase of atmospheric moisture in a warmer climate. If one ignores changes in atmospheric circulation, the moisture flux convergence in regions with climatological convergence tends to increase as moisture increases and then enhances the corresponding precipitation (Chou and Neelin, 2004; Held and Soden, 2006; Chou et al., 2009). The warmer-get-wetter pattern involves precipitation increases in places where the rise in sea surface temperature (SST) exceeds the mean surface warming of the tropics (Xie et al., 2010; Chadwick et al., 2013). A recent study showed that both the wet-get-wetter and warmer-get-wetter mechanisms are important for tropical precipitation change, dominating the annual mean and seasonal anomalies, respectively (Huang et al., 2013).

Precipitation change has a strong seasonal dependence because of the strong seasonal cycle of atmospheric circulation (Seager et al., 2010; Noake et al., 2012; Polson et al., 2013). Coupled climate model simulations show that the globally averaged annual range (AR) of precipitation tends to increase under global warming, and the increase largely comes from moistening of the wet season (Chou and Lan, 2012). Such changes have been detected in observations, especially over the past few decades (Chou et al., 2013). However, studies on the seasonal precipitation change in a warming climate remain quite limited.

Climate system models (CSMs) play an instrumental role in understanding and simulating past, present and future climates. The State Key Laboratory of Numerical Modeling for Atmospheric Sciences and Geophysical Fluid Dynamics, Institute of Atmospheric Physics, Chinese Academy of Sciences (LASG/IAP/CAS) has devoted great efforts to the development of component models and fully coupled models (see Zhou et al., 2007, 2014). New versions of the Flexible Global Ocean–Atmosphere–Land System model (FGOALS) have been established and are participating in the ongoing Coupled Model Intercomparison Project Phase 5 (CMIP5) experiments. Two versions of the FGOALS model, FGOALS-g2 and FGOALS-s2, share the same coupling framework, ocean and land components, but adopt different atmospheric and sea ice components (Bao et al., 2013; Li et al., 2013). Confidence in model projection is closely related to the ability to simulate the recent climate and climate changes with sufficient realism. The performances of the FGOALS models in simulating major climate phenomena, e.g. annual SST cycles and the 20th century global and regional surface air temperature changes, ENSO–monsoon relationship, and global monsoons, have been assessed (Li et al., 2013; Bao et al., 2013; Wu and Zhou, 2013; Zhou et al., 2013a; Zhang and Zhou, 2014). However, the performance of FGOALS in the simulation of seasonal precipitation changes in wet and dry seasons during the past century have never been assessed.

The current study aims to evaluate the performance of the LASG/IAP model in the simulation of seasonal precipitation. The following questions are addressed: (1) How well do the two versions of FGOALS simulate the mean state of the timing of the wet and dry seasons and related precipitation amounts? (2) What are the characteristics of precipitation change in the wet and dry seasons, especially the AR, during the 20th century in the historical climate simulations performed by the FGOALS models? (3) What are the mechanisms responsible for precipitation change in the wet and dry seasons? Since the long-term change of global precipitation in 20th century historical climate simulations is dominated by the responses of the coupled system to greenhouse gas forcing, and many ocean–atmosphere feedback processes are involved, only fully coupled climate models can be used in this kind of diagnosis (Xie et al., 2010; Chou and Lan, 2012; Chadwick et al., 2013).

2. Model, data and analysis method

2.1. *Model, experiments and data description*

Both FGOALS-g2 and FGOALS-s2 are composed of four interactive component models, including atmospheric, oceanic, land and sea ice models that are coupled together by the National Center for Atmospheric Research's flux coupler module, version 6 (CPL6). These two versions of FGOALS share the same ocean and land component models, but differ in their atmospheric and sea ice components. The ocean component of FGOALS is the LASG/IAP's Climate System Ocean Model version 2 (LICOM2), which has a horizontal resolution of about $1^\circ \times 1^\circ$ in the extratropical zone and $0.5^\circ \times 0.5^\circ$ in the tropics, and 30 vertical levels. The land component is the Community Land Model version 3 (CLM3). For FGOALS-s2, the atmospheric component is the Spectral Atmospheric Model of the IAP/LASG version 2 (SAMIL2), with a horizontal resolution of about 2.81° (lon) $\times 1.66^\circ$ (lat) and 26 levels in the vertical direction; the sea ice component is the Community Sea Ice Model version 5 (CSIM5) (Bao et al., 2013). In FGOALS-g2, the atmospheric component is the Grid-point Atmospheric Model of the IAP/LASG version 2 (GAMIL2), with a horizontal resolution of about $2.8^\circ \times 2.8^\circ$ and 26 levels in the vertical direction; the sea ice component is the Los Alamos Sea Ice Model (CICE) (Li et al., 2013). For more detailed information about these two model versions, readers are referred to Bao et al. (2013) and Li et al. (2013).

In this study, the outputs of the 20th century historical climate simulations and pre-industrial control simulations (PI

control) by the two versions of FGOALS are diagnosed. The 20th century historical climate simulation is a standard experiment of CMIP in which the models are forced by various and identical historical atmospheric forcing agents recommended by CMIP (Zhou and Yu, 2006). The PI control run integrated starting from the equilibrium state of a standalone 500-yr spin-up integration of LICOM2. The values of external forcing agents in the PI control run were fixed at the level of the year 1850 (Bao et al., 2013; Li et al., 2013). More details of the experiment design can be found Taylor et al. (2012). In addition, the monthly mean precipitation from the Global Precipitation Climatology Project (GPCP) (Adler et al., 2003) is used as the observational evidence to gauge the model performance.

2.2. *Analysis method*

The wet season, also called the rainy season, is an annually recurring period of one or more months during which precipitation is at a maximum for that region; the opposite is the dry season. In previous studies, the AR of precipitation has been defined as the local summer-minus-winter precipitation, with summer meaning June–July–August (JJA) in the Northern Hemisphere (NH) and December–January–February (DJF) in the Southern Hemisphere (SH) (Wang and Ding, 2006; Zhou et al., 2008). So, the NH (SH) share the same and fixed occurrence times of the wet (dry) season everywhere.

In fact, the timings of the wet and dry seasons are strongly dependent on geographic location. In addition, the wet and dry seasons could shift under global warming. Trenberth et al. (2003) suggested that the liquid-precipitation season has become longer by up to 3 weeks in some regions of the boreal high latitudes over the last 50 years, owing to an earlier onset of spring. Over the United States, from 1930 to 2009, the day of the year on which certain percentiles of annual total precipitation were achieved indicated spatially coherent patterns of change; regionally consistent trends in the timing of wet (dry) seasons were also evident, particularly over the Ohio (Missouri) River valleys where the dry season arrived up to 2–3 weeks earlier (later) (Pryor and Schoof, 2008). The same phenomena have been found in other studies (Pal et al., 2013). So, fixed wet and dry seasons do not necessarily delineate the timing of wet and dry season precipitation at a particular station and the changes therein.

Recognizing the changing behavior of the timing of wet and dry seasons, in our study we define the AR as the precipitation difference between the wet and the dry season in each year and at each grid or station, following Chou et al. (2013). The wet (dry) season is defined as an annually recurring period of 3 months during which precipitation is maximum (minimum) for that grid, and the central point of the 3 months is used to denote the timing of the wet or dry season. So, the timing of the wet (dry) season varies temporally and spatially.

In the analysis, we first convert the monthly products of the observed and simulated fields to seasonal variables, using 3-month running averages. Then, the maximum values of seasonal precipitation for each grid and each year are calculated and referred to as the wet-season precipitation amount of that grid and that year. The time when the maximum seasonal precipitation occurs for each grid and each year is the occurrence time of the wet season for that grid and that year. Corresponding strictly to the wet season of each grid and each year, values of related climate variables, e.g. evaporation, vector winds and specific humidity, of that grid and that year are extracted. The above wet-season data processing is also applied to the dry season, which is based on the minimum values of seasonal precipitation. The area-weighted averages are calculated for the global regions. Resultant globally averaged wet (dry) season precipitation means the global probable maximum (minimum) seasonal precipitation amount. The resultant wet (dry) season evaporation is the evaporation amount when precipitation reaches its seasonal maximum (minimum). As the wet and dry season varies from grid to grid and year to year, the resultant globally averaged convergence of moisture flux cannot be zero. Thus, the global mean wet (dry) season precipitation cannot be balanced by the global mean wet (dry) season evaporation. Here, the climatology is calculated for the period 1979–2005.

In order to understand the mechanisms responsible for precipitation changes in the wet and dry season and the AR, as in previous studies (Held and Soden, 2006; Seager et al., 2010; Chou and Lan, 2012; Huang et al., 2013) we start from the vertically integrated moisture equation, which can be written as

$$P = -\partial_t\langle q\rangle - \langle\nabla\cdot\boldsymbol{V}q\rangle + E + \delta\ , \tag{1}$$

where P is precipitation, E is evaporation and $\boldsymbol{V}$ is vector wind. The symbol $\langle\rangle$ means a mass integration through the entire troposphere. All values in Eq. (1) are seasonally averaged. $\partial_t\langle q\rangle$ is the time derivative of specific humidity $q$and can generally be ignored as its seasonal mean value is much smaller than that of other terms. $-\langle\nabla\cdot\boldsymbol{V}q\rangle$ is the convergence of moisture flux. δ is a residual term, which includes transient eddies (water vapor transport at the sub-seasonal time scale) and contributions from surface processes due to topography (Seager et al., 2010). Based on the mass conservation equation, i.e. $\nabla\cdot\boldsymbol{V} = 0$ and following Chou et al. (2009, 2013) and Chou and Lan (2012), the convergence of moisture flux $-\langle\nabla\cdot\boldsymbol{V}q\rangle$ can be divided into two terms: vertical moisture advection$-\langle\omega\partial_p q\rangle$ and horizontal moisture advection $-\langle\boldsymbol{V}_h\cdot\nabla_h q\rangle$. ∇_h is the horizontal differential operator. Equation (1) can then be approximately written as

$$P \approx -\langle\omega\partial_p q\rangle - \langle\boldsymbol{V}_h\cdot\nabla_h q\rangle + E + \delta\ , \tag{2}$$

where the subscripts "p" and "h" denote pressure and horizontal direction, respectively. ω is pressure velocity and $\boldsymbol{V}_h$ is horizontal vector wind. Vertical moisture advection $-\langle\omega\partial_p q\rangle$ is the part of the convergence of moisture flux induced by vertical motion. If the pressure velocity ω is assumed to be zero at the surface and at the tropopause, we get $\langle\partial_p\omega q\rangle = 0$ and $-\langle\omega\partial_p q\rangle = -\langle q\nabla_h\cdot\boldsymbol{V}_h\rangle$. So, the vertical moisture advection is also referred to as the horizontal flow convergence of the

moisture term (Seager et al., 2010). Note that the vertical moisture advection is associated with the low-level convergence; the low-level convergence can promote the upward transport of moisture and then can greatly speed up the rain formation.

According to Eq. (2), we can decompose the precipitation changes into

$$P' \approx -\langle \omega \partial_{\rm p} q \rangle' - \langle \boldsymbol{V}_{\rm h} \cdot \nabla_{\rm h} q \rangle' + E' + \delta' \ . \qquad (3)$$

Here, primes indicate departures from the climatology. As any dependent variable can be divided into a constant basic state portion (denoted by an overbar) and a perturbation portion (denoted by a prime), so the pressure velocity ω and the specific humidity q can be described as follows: $\omega = \overline{\omega} + \omega'$; $q = \overline{q} + q'$. Changes of the vertical moisture advection $-\langle \omega \partial_{\rm p} q \rangle$ can be further approximated as

$$-\langle \omega \partial_{\rm p} q \rangle' = -\langle \overline{\omega} \partial_{\rm p} q' \rangle - \langle \omega' \partial_{\rm p} \overline{q} \rangle - \langle \omega' \partial_{\rm p} q' \rangle \ . \qquad (4)$$

The atmospheric boundary layer contains the bulk of column-integrated atmospheric water. Boundary layer specific humidity is constrained by the surface energy balance to increase with temperature approximately following the Clausius–Clapeyron relation (Boer, 1993; Held and Soden, 2000). The first term on the right of Eq. (4) only involves changes in specific humidity q but no changes in pressure velocity ω; the second term only involves changes in pressure velocity ω but no changes in specific humidity q. In other words, $-\langle \overline{\omega} \partial_{\rm p} q' \rangle$ is associated with changes in water vapor, which is mainly induced by temperature changes; $-\langle \omega' \partial_{\rm p} \overline{q} \rangle$ is associated with changes in pressure velocity, which is mainly induced by atmospheric circulation changes. Following previous studies (Chou and Lan, 2012; Chou et al., 2013; Huang et al., 2013), $-\langle \overline{\omega} \partial_{\rm p} q' \rangle$ is termed the thermodynamic component and $-\langle \omega' \partial_{\rm p} \overline{q} \rangle$ is termed the dynamic component of $-\langle \omega \partial_{\rm p} q \rangle'$. The last term on the right of Eq. (4) is the nonlinear term that is the product of changes both in vertical pressure velocity ω and water vapor q. As the contribution of horizontal moisture advection to precipitation changes is relatively small, it is not divided into the thermodynamic component and dynamic component as is the case for vertical moisture advection. So, as in previous studies (Chou et al., 2009; Chou and Lan, 2012; Chou et al., 2013; Huang et al., 2013), in this study the thermodynamic and dynamic component refers specifically to $-\langle \overline{\omega} \partial_{\rm p} q' \rangle$ and $-\langle \omega \partial_{\rm p} q \rangle'$, respectively. Unlike in Seager et al. (2010), thermodynamic contributors refer to all changes in specific humidity q but no changes in wind $\boldsymbol{V}$ on the right side of Eq. (3), and dynamic contributors refer to all changes in $\boldsymbol{V}$ but no changes in q.

3. Results

In the following analysis we first examine the performance of the two versions of FGOALS in reproducing the spatial distribution of the timing of the climatological wet and dry seasons. We also examine the climatology of the precipitation of the wet and dry seasons, and the AR, in models by comparing their results with observations. We then evaluate the precipitation change in the wet and dry seasons of the 20th century historical climate simulations. The changes in AR are also analyzed. Finally, the possible mechanisms responsible for the changes of seasonal precipitation are discussed.

3.1. *Climatological mean state*

The climatological wet (dry) season is defined as three consecutive months during which precipitation reaches its maximum (minimum) based on the climatological 12-month mean precipitation. The climatological spatial distributions of the timings of the wet and dry seasons, which are derived from observations and the simulations of FGOALS-g2 and FGOALS-s2, are shown in Fig. 1.The observations are dominated by two features. First, generally, the wet season is mainly in the summer–autumn months, while the dry season is mainly in the winter–spring months (Figs. 1a and b). Second, substantial spatial features are evident in the occurrence of the climatological wet and dry seasons. In northwestern Europe, most of Asia, small areas of northwestern North America, the South China Sea, southern Africa, northern Australia, parts of the southern tropical Pacific, and Central America, the wet season mainly occurs in summer and the dry season mainly in winter. Autumn is the timing of the wet season in most parts of the tropical Atlantic. The wet season occurs in July–August–September (JAS) (one month later than boreal summer) in the Arctic Ocean. The wet and dry seasons over the subtropical oceans tend to start from the winter and summer months, respectively. Autumn corresponds to the wet season in the Southern Ocean.

The timings of the climatological wet and dry seasons in the two models show spatial patterns that are similar to those in the observations (Figs. 1c–f), but some biases are also evident. The largest deficiency is a delayed occurrence of the wet and dry seasons in most global regions in the two models (Fig. 2). However, regional details are different. In FGOALS-g2, the start of the wet or dry season is earlier than in the observation in most of the high latitudes, but later in most of the middle and low latitudes (Figs. 2a and c). In FGOALS-s2, over the Arctic, northern Europe, extensions of the western boundary currents, the equatorial Pacific, and the Gulf of Mexico, both the wet and dry seasons start later than in the observations. In northern Asia, the wet season starts later but the dry season starts earlier than in observations (Figs. 2b and d).

To quantitatively evaluate the models' performances in their simulations of the timing of the climatological wet and dry seasons, the weighted pattern correlation coefficient (PCC), root-mean-square difference (RMSD) and standard deviation ratio (SDR) of the occurrence time of the climatological wet and dry seasons between the models and observation are calculated. For the wet season, FGOALS-g2 and FGOALS-s2 both show a PCC of 0.65, which is statistically significant at the 1% level. The standard deviations of the simulations in both models are larger than that in the observation, and SDRs are also the same at 1.05. The RMSD is

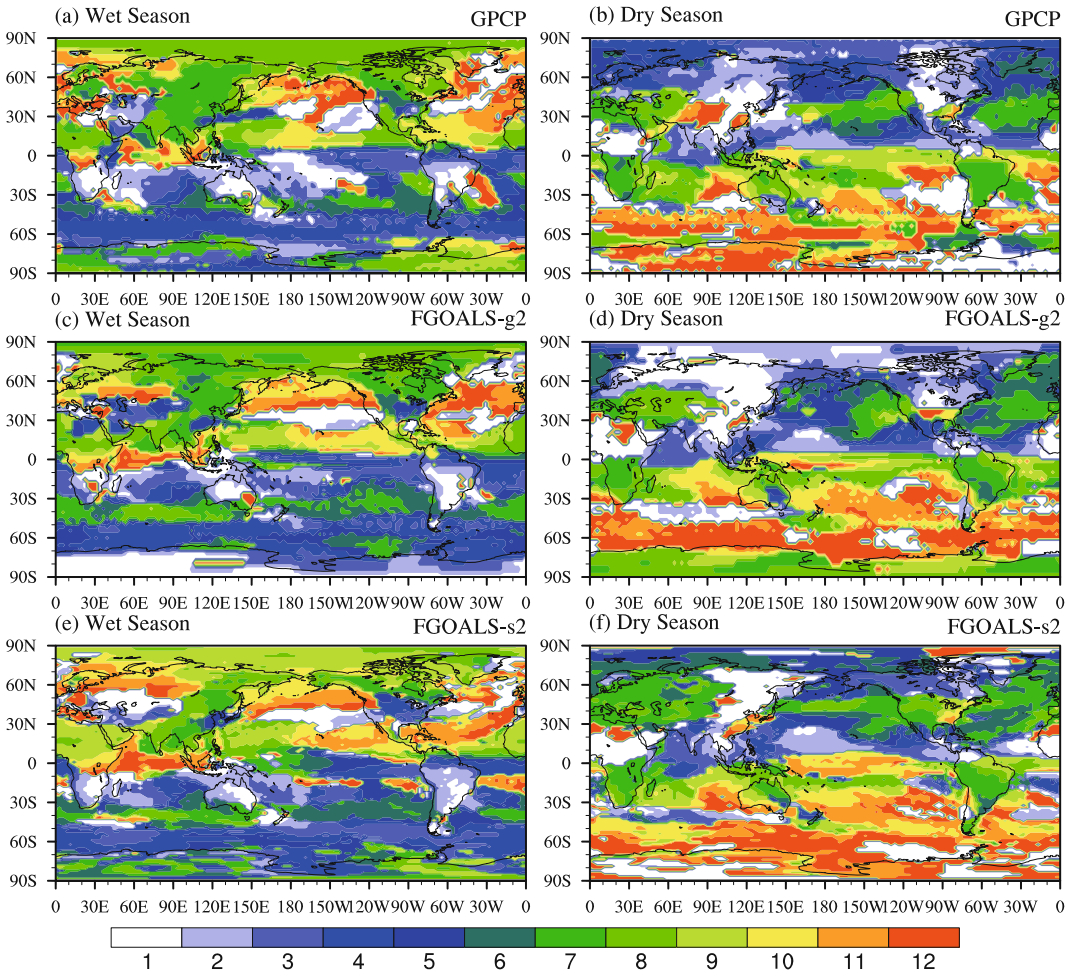

Fig. 1. Timing of the (a, c, e) climatological wet season and (b, d, f) dry season from (a, b) observations, (c, d) FGOALS-g2 and (e, f) FGOALS-s2. The numbers 1 to 12 in the color bar indicate the time that the wet and dry seasons occur, 1: DJF (Dec–Feb); 2: JFM (Jan–Mar); 3: FMA (Feb–Apr); 4: MAM (Mar–May); 5: AMJ (Apr–Jun); 6: MJJ (May–Jul); 7: JJA (Jun–Aug); 8: JAS (Jul–Sep); 9: ASO (Aug–Oct); 10: SON (Sep–Nov); 11: OND (Oct–Dec); 12: NDJ (Nov–Jan).

2.11 in FGOALS-g2 and 2.31 in FGOALS-s2. The abilities of FGOALS-g2 and FGOALS-s2 in reproducing the mean occurrence of the wet season are equivalent. For the dry season, compared to FGOALS-s2, FGOALS-g2 has a larger PCC and SDR: the PCC is 0.66 in FGOALS-g2 and 0.63 in FGOALS-s2, both of which are statistically significant at the 1% level; the SDR (RMSD) is 1.12 (2.24) in FGOALS-g2 and 1.03 (2.38) in FGOALS-s2. Therefore, on the whole, both FGOALS-g2 and FGOALS-s2 can reasonably simulate the mean timings of the wet and dry seasons.

But how well do the two versions of FGOALS simulate the climatology of seasonal precipitation? Figure 3 shows the spatial distributions of climatological precipitation in the wet and dry seasons. For the wet season, observed values of precipitation vary spatially from less than 0.2 mm d^{-1} or to a maximum of more than 14 mm d^{-1} (Fig. 3a). The distribution of precipitation is similar to the annual mean precipitation (figure not shown). Precipitation is dominated by atmospheric circulation, surface temperature and water vapor conditions. Therefore, the distribution of precipitation in the wet season has features as follows. Deserts are evident in the subtropical regions. Dry regions are seen in continental areas and polar areas. The areas near the equator receive high amounts of precipitation. Precipitation has a secondary maximum over the North Pacific and Atlantic oceans.

The climatological wet season precipitation in the two models has a spatial pattern similar to that of GPCP, with a PCC of 0.84 (0.83), RMSD of 2.03 (2.10), and SDR of 1.10 (1.11) for FGOALS-g2 (FGOALS-s2). However, biases are still evident. In the tropical regions, stronger precipitation over the western Indian and central Pacific near the equator is evident in the two model versions (Figs. 3c and e). There are clear double Intertropical Convergence Zone (ITCZ) structures about the simulated climatological wet season precipitation in the two versions of the FGOALS model. Precipitation over South America and northeastern Europe is underestimated in both models.

In the dry season, except for specific regions such as the ITCZ, South Pacific Convergence Zone (SPCZ), equatorial Indian and Amazon, precipitation is weak over the entire

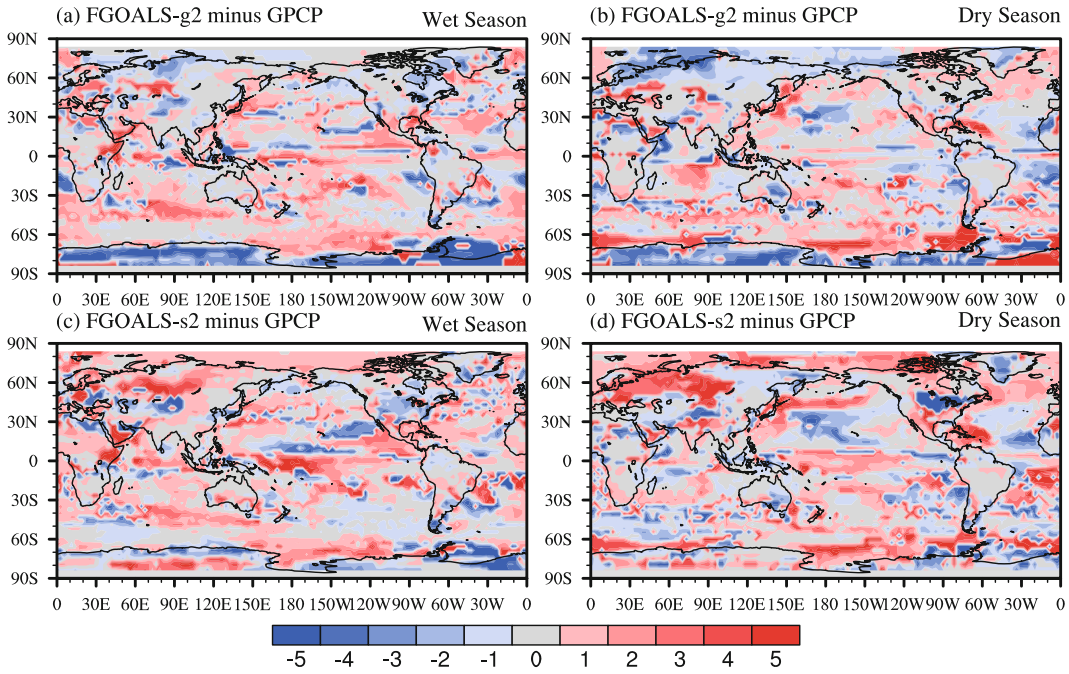

Fig. 2. The difference in the timing of the climatological wet and dry seasons between the models and observations: (a, b) FGOALS-g2 minus GPCP; (c, d) FGOALS-s2 minus GPCP; (a, c) wet season; (b, d) dry season. Units: months.

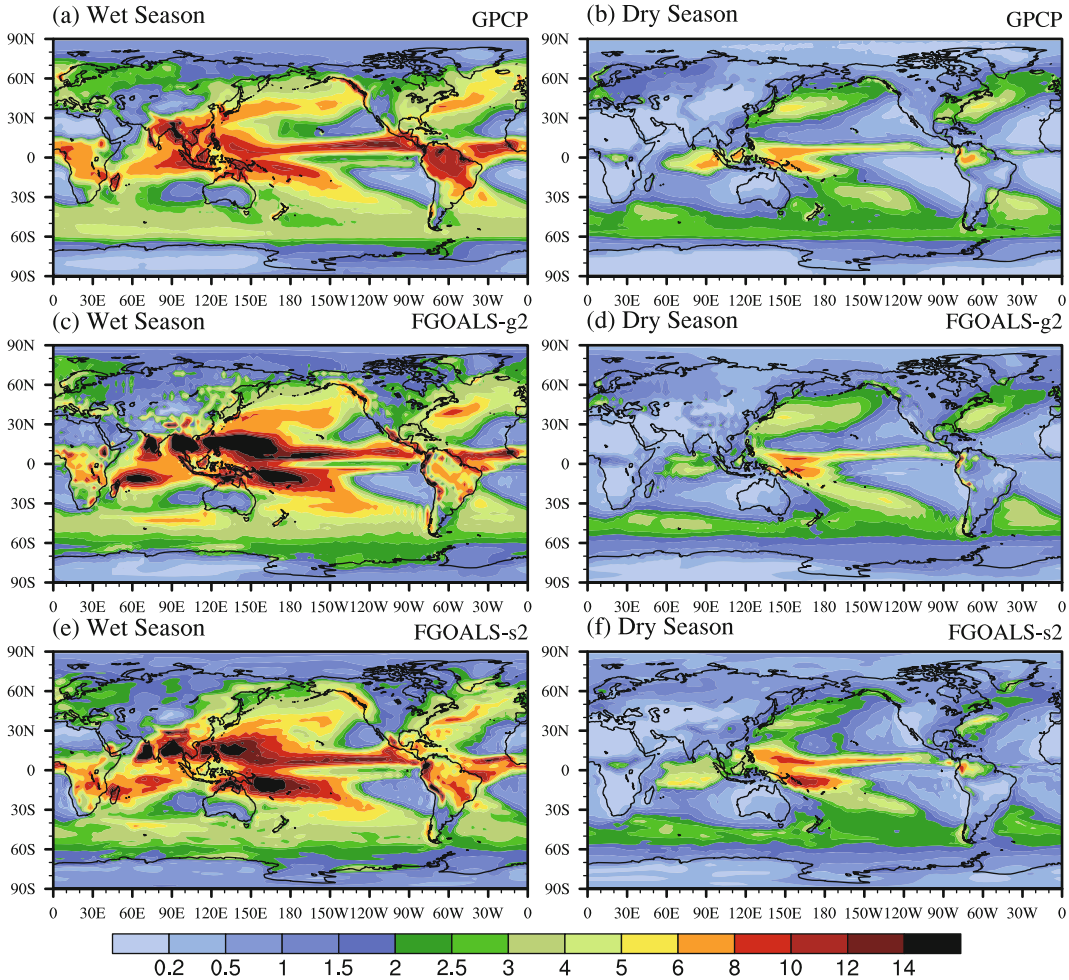

Fig. 3. Climatological precipitation of the (a, c, e) wet season and (b, d, f) dry season based on (a, b) observations, (c, d) FGOALS-g2 and (e, f) FGOALS-s2. Units: mm d^{-1}.

globe (Figs. 3b, d and f). The PCC between the simulation and observation is 0.84 (0.83) for FGOALS-g2 (FGOALS-s2). The corresponding SDR is 0.96 (1.08) and RMSD is 2.03 (2.11) for FGOALS-g2 (FGOALS-s2). Both models overestimate the precipitation over the ITCZ and SPCZ with a double ITCZ structure, but underestimate the precipitation over the midlatitude Atlantic and the northern Pacific.

The observed and simulated spatial distributions of the climatological AR of precipitation are shown in Fig. 4. The maximum centers of AR are mainly located in or near the boundary between the sea and land. Over the equatorial Atlantic, Amazon and equatorial Africa, the maximums of AR are evident. The PCC, RMSD and SDR is 0.81, 1.78 and 1.11 (0.80, 1.79 and 1.09) for FGOALS-g2 (FGOALS-s2), respectively. A larger AR over the central equatorial Pacific and Indian oceans is simulated in the two models.

There are clear double ITCZ structures in the two coupled versions of FGOALS. However, the contribution of the spurious ITCZ in the SH to globally averaged precipitation is limited. Previous studies have demonstrated that if coupled climate models demonstrate reasonable performance in reproducing the mean state of global precipitation, the double ITCZ problem cannot prevent us from examining global precipitation change and discussing related dynamical causes through using these models, and thus they have been widely used in studies of global precipitation changes (Held and Soden, 2006; Seager et al., 2010; Chou and Lan, 2012; Huang et al., 2013). Chapter 9 of the *Intergovernmental Panel on Climate Change Fifth Assessment Report* (IPCC AR5) states that the mean state biases do not obviously affect the modeled response to greenhouse gas forcing (Flato et al., 2013). The above assessment indicates reasonable performance of the two versions of FGOALS in reproducing the timing of climatological wet and dry seasons and related precipitation amounts. This forms a solid base for our analysis in the following two sections of the seasonal precipitation response to global warming in the 20th century as simulated by FGOALS.

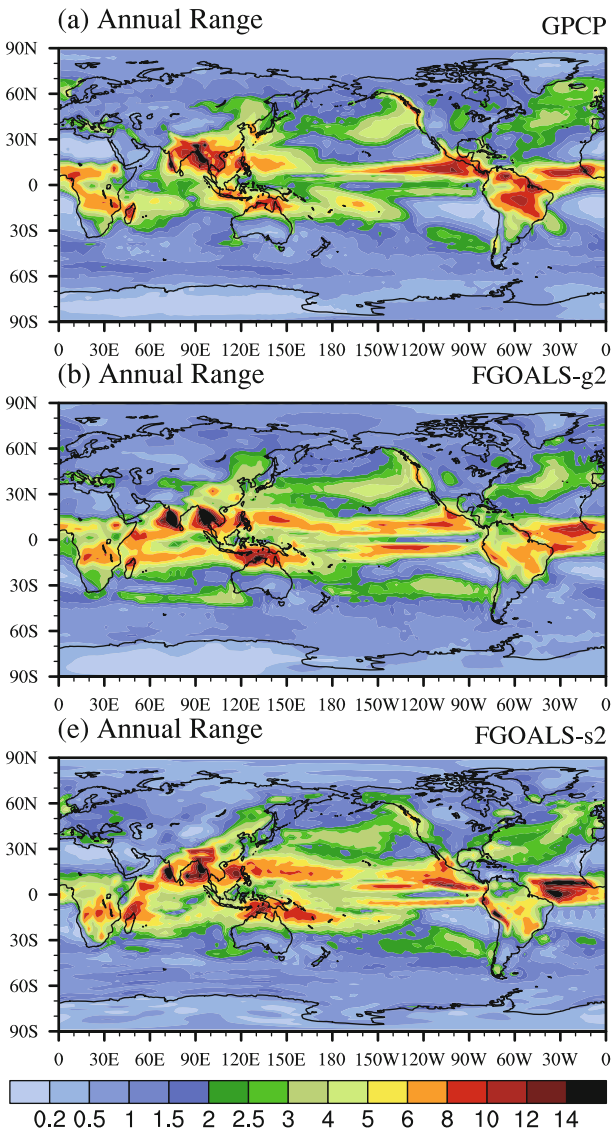

Fig. 4. As in Fig. 3 except for the annual range of precipitation.

3.2. *Precipitation changes in the 20th century*

To assess the impact of global warming on the hydrological cycle, records longer than 100 years are required (Vecchi et al., 2006). For periods shorter than 100 years, it is very likely that the multi-decadal internal variability dominates the long-term trend. However, observational data on global precipitation are only available from 1979 (Adler et al., 2003), and the 20th century historical simulations of FGOALS-g2 and FGOALS-s2 only cover 1850–2005. Therefore, simulated temporal evolutions of global mean precipitation in the wet and dry seasons, and the AR, during 1850–2005 are plotted against the observations during 1979–2012 in Fig. 5. The observation and model results are both normalized by their climatological mean. In the observations, the mean value of globally averaged precipitation for the wet season is 4.5488 mm d^{-1}. For the dry season the value is 1.2407 mm d^{-1}, and the AR is 3.3080 mm d^{-1}. In FGOALS-g2 (FGOALS-s2), the mean value of globally averaged precipitation for the wet season, dry season and AR is 4.9058, 1.2840 and 3.6219 (4.8711, 1.1203 and 3.7508) mm d^{-1}, respectively. For the wet season, the globally averaged precipitation in both observation and model results show significant upward trends, with rates of 0.2576 mm d^{-1} (34 yr)$^{-1}$, 0.0491 and 0.2051 mm d^{-1} (156 yr)$^{-1}$ for GPCP, FGOALS-g2 and FGOALS-s2, respectively. All these trends exceed the 99% confidence level of the Student's *t*-test. Note that PI control simulations can be used as an indicator of natural variability without anthropogenic impacts. Based on the PI control simulations of both models, we estimate that the width of the 95% confidence interval of the 156-year trend is $\pm$0.0245 (0.0351) mm d^{-1} (156 yr)$^{-1}$ for FGOALS-g2 (FGOALS-s2). Therefore, this upward trend of maximum precipitation is mainly the model response to external forcing rather than internal variability.

For the dry season, observations show a drying trend over the last three decades with a rate of -0.1699 mm d^{-1} (34 yr)$^{-1}$, which is statistically significant at the 1% level. Chou

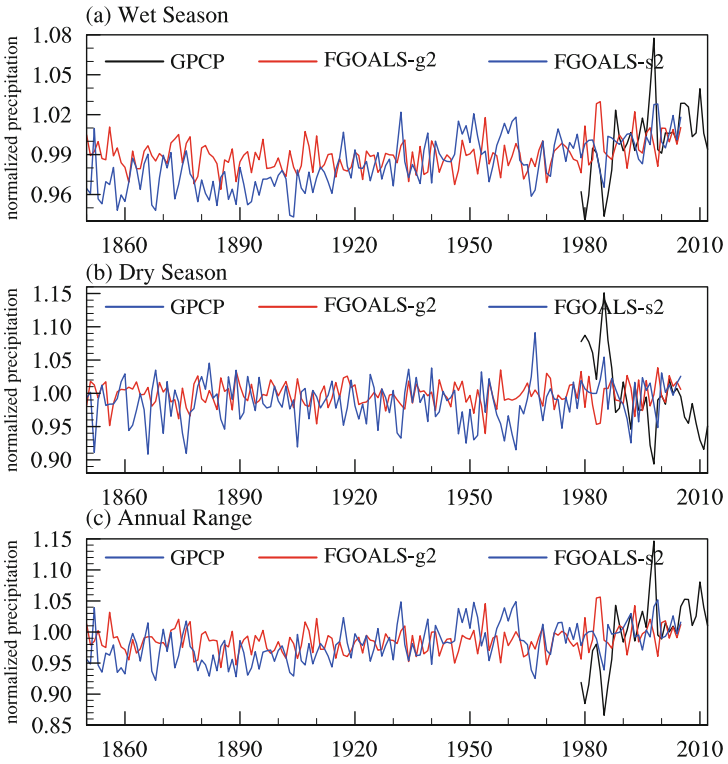

Fig. 5. Time series of globally averaged precipitation during the 20th century, normalized to units by the mean over 1979–2005: (a) wet season; (b) dry season; (c) annual range. Black lines correspond to the observational records of the GPCP over 1979–2012; red and blue lines correspond to the 20th century historical simulations for the period 1850–2005 of FGOALS-g2 and FGOALS-s2, respectively.

et al. (2013) found that the sign of precipitation tendency for the dry season is inconsistent among different observational data. Hence, caution should be applied to this observed drying trend. The trend of globally averaged precipitation in the dry season is positive in both models, with a rate of 0.0017 (0.0115) mm d^{-1} $(156\ yr)^{-1}$ for FGOALS-g2 (FGOALS-s2), but both are statistically insignificant at the 5% level.

It is evident that the magnitude of precipitation change in the wet season is stronger than that in the dry season in both observations and the model simulations. As a result, the AR of precipitation increases significantly. Importantly, the observed wetter wet season and drier dry season combine to enhance the AR. However, in both FGOALS-g2 and FGOALS-s2, the simulated moistening of the dry season offsets the contribution of the wetter wet season in terms of the simulated increase of the AR. The observed increasing trend of the AR over 1979–2012 is 0.4275 mm d^{-1} $(34\ yr)^{-1}$. The simulated increasing trend of the AR over 1850–2005 is 0.0474 (0.1936) mm d^{-1} $(156\ yr)^{-1}$ for FGOALS-g2 (FGOALS-s2). All of these three trends are statistically significant at the 1% level.

The signs of the globally averaged precipitation trend for the wet season and the AR are consistent between the observations and simulations. However, the trends derived from the observations are larger than those derived from the simulations. This phenomenon is also evident in other models (Allan et al., 2010; Chou et al., 2013; Polson et al., 2013). Nevertheless, the reasons responsible for the discrepancy remain unknown. One possible explanation is that the time span of three decades for the observational record is too short to distinguish the effect of GHG-forced global warming from natural variability. For detection periods shorter than 100 years, it is very likely that the decadal internal variability, such as mega ENSO, Pacific Decadal Oscillation (PDO) or Interdecadal Pacific Oscillation (IPO) events, dominates the long-term changes of the coupled climate system (Vecchi et al., 2006). In fact, recent studies have demonstrated that mega-ENSO (a leading mode of interannual-to-interdecadal variation of global SST) and the Atlantic Multidecadal Oscillation have intensified the global monsoon precipitation during the most recent three decades (Wang et al., 2012, 2013). The changes of the East Asian summer monsoon (EASM) precipitation are largely dominated by natural internal variability of the PDO, resulting in the EASM exhibiting no significant long-term trend during the 20th century (Zhou et al., 2009; Li et al., 2010; Zhou et al., 2013b; Qian and Zhou, 2014). As the phase of the multi-decadal mode in coupled models is not in sync with those in observations, and the natural decadal variability in the two versions of FGOALS during the 20th century may be weaker than that in observations,

the observed trend magnitude is larger than those simulated by FGOALS-g2 and FGOALS-s2. Another possible explanation is that there are errors in observational records, which may lead to a spuriously large observed trend (Allan et al., 2010).

Regardless of whether for the wet season, dry season, or AR, the linear trend of the globally averaged precipitation in FGOALS-g2 during 1850–2005 is smaller than that simulated by FGOALS-s2. This discrepancy may be related to the model's sensitivity to the external radiative forcing. FGOALS-s2 has a larger climate sensitivity (4.5 K), defined as the equilibrium temperature change under double CO_2 forcing, than FGOALS-g2 (3.7 K) (Chen et al., 2014). Zhou et al. (2013a) examined the historical evolution of global surface air temperature simulated by FGOALS-g2 and FGOALS-s2 during 1850–2005 and suggested that FGOALS-s2 has a stronger response to anthropogenic forcing, because the sea-ice albedo feedback and water vapor feedback in FGOALS-s2 is stronger than those in FGOALS-g2.

We further examine the spatial pattern of the precipitation trends in the wet and dry seasons in the 20th century historical simulations. To better capture the regional features of precipitation change, the climatological wet- and dry-season mean precipitation values are sorted by intensity among all grids of the models and observations. We then divide the sorted precipitation into 20 percentile bins. The interval of each percentile bin is 5%. The value in each bin is the area-weighted average of those areas having the corresponding level of precipitation intensity. For example, the first and the last bins

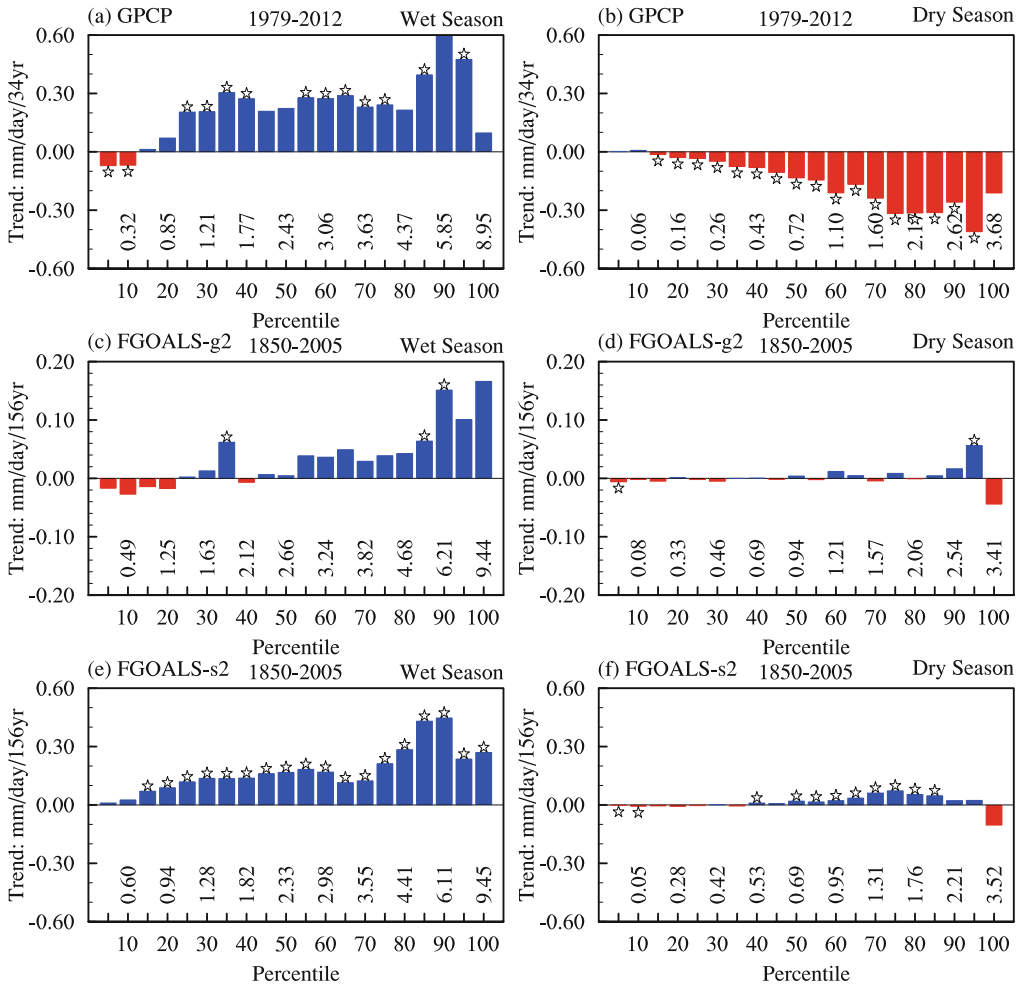

Fig. 6. The observed (1979–2012) and simulated (1850–2005) changes in precipitation amount calculated from linear regression: (a, b) GPCP; (c, d) FGOALS-g2; (e, f) FGOALS-s2; (a, c, e) wet season; (b, d, f) dry season. The interval of each percentile bin is 5%. Red and blue bars indicate positive and negative trends, respectively. Stars denote that the trend is statistically significant at the 95% confidence level. The *y*-axis is the linear trend; the *x*-axis is the percentile rank (%). The values labeled vertically are the wet- and dry-season mean precipitation intensities (mm d^{-1}) for the period 1979–2005 at the lower bounds of each 5% percentile bin.

denote the areas with the lowest and highest climatological wet- or dry-season mean precipitation amount, respectively.

Figure 6 shows the corresponding precipitation trend of each bin in the wet and dry seasons. In the wet season, in both the observations and models, most regions of the world get wetter, while some regions with low climatological wet-season rainfall get drier. In the dry season, observations show a mostly significant drying trend, except for regions with low climatological dry-season precipitation, and the amplitude of the drying tendency is comparable to the change in the wet season. However, the simulated patterns of dry-season precipitation change are different from those observed. A drying of the dry season is seen in most regions of the world in the observations. Drier dry seasons in the two models only occur in those regions with the lowest or highest climatological dry-season mean precipitation amount, and the trends are smaller than those of the wet season. The change in the AR distribution is similar to the change in the precipitation of the wet season (figure not shown).

3.3. *Moisture budget analysis and mechanisms*

In this section, to understand which specific processes are responsible for the changes of precipitation in the wet and dry seasons and the AR, we examine the vertically integrated moisture budget equation shown in Eq. (3). According to Eq. (3), the rainfall changes are caused mainly by the sum of changes in vertical moisture advection, horizontal moisture advection and surface evaporation.

From the climate mean state, regardless of the season, globally averaged rainfall is balanced mainly by the evaporation and vertical moisture advection, whereas the contributions of horizontal moisture advection and the residual are relatively small (Fig. 7). The results of both models indicate that the contributions of evaporation and the convergence of moisture flux (including vertical and horizontal moisture advection) are positive in the wet season and for the AR. For dry season, however, the convergence of moisture flux is unfavorable for precipitation.

The time series of the moisture budget associated with precipitation in the wet season is shown in Fig. 8. In FGOALS-g2, evaporation increases at a rate of 0.0204 mm d^{-1} (156 yr)$^{-1}$, which is statistically significant at the 1% level; vertical moisture increases at a rate of 0.0249 mm d^{-1} (156 yr)$^{-1}$, which is only statistically significant at the 10% level (Figs. 8a and b, Table 1). In FGOALS-s2, evaporation and vertical moisture advection show increasing trends of 0.0550 and 0.1675 mm d^{-1} (156 yr)$^{-1}$, both of which are statistically significant at the 1% level. The horizontal mois-

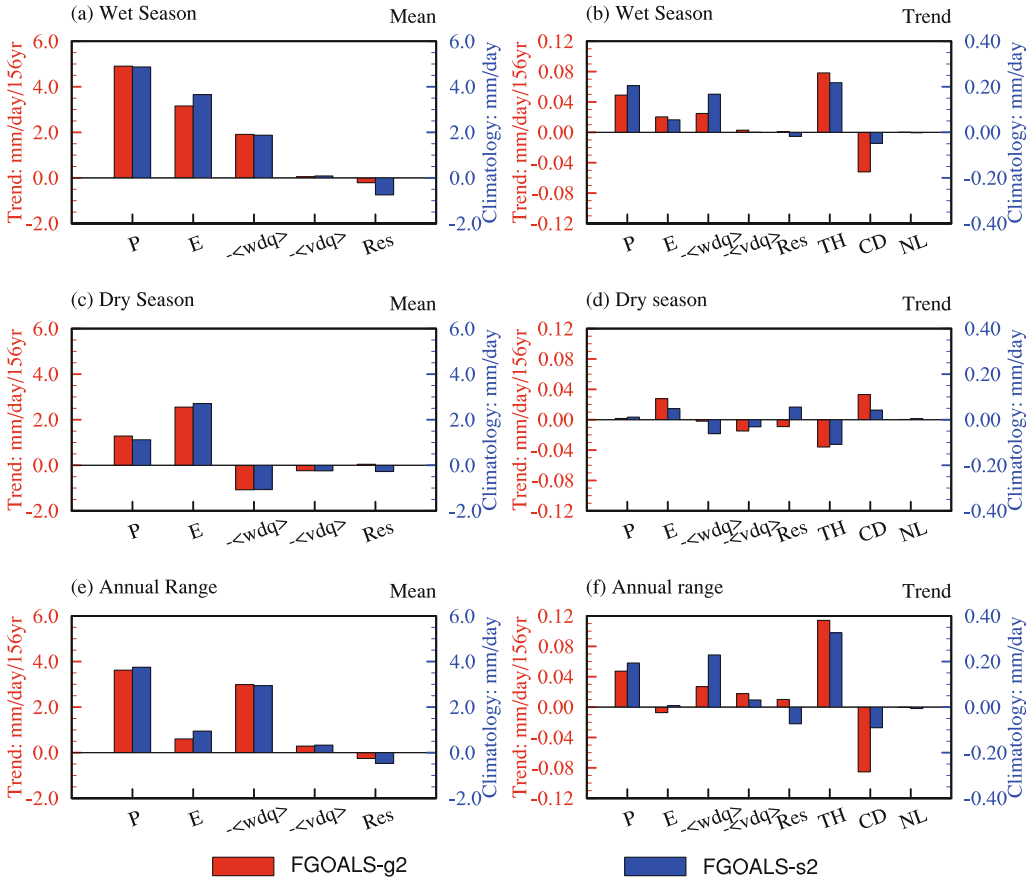

Fig. 7. The (a, c, e) climatology (units: mm d^{-1}) and (b, d, f) trends [units: mm d^{-1} (156 yr)$^{-1}$] of globally averaged precipitation and moisture budget terms in the (a, b) wet season, (c, d) dry season, and (e, f) annual range. Red (blue) coloring and the left (right) axis corresponds to FGOALS-g2 (FGOALS-s2).

ture advection and the residual show no obvious trends (Figs. 8c and d). Among the different contributions to the wetter wet–season trend, more than half comes from the vertical advection, while the remaining contribution mainly comes from evaporation (Fig. 7b). In other words, vertical moisture advection is the most important process in forming the wetter wet season.

We further examine the changes in the thermodynamic and dynamic components, i.e. the first and second terms on the right of Eq. (4). The thermodynamic and dynamic components are closely correlated to the precipitable water and vertical pressure velocity. The change in precipitable water vapor and vertical velocity at 500 hPa are also diagnosed. Both the water vapor and the vertical pressure velocity show significantly upward trends (Figs. 8g and h), indicating that globally averaged water vapor increases and the circulation weakens as the global climate warms up. As a result, the thermodynamic component shows a significantly positive trend at a rate of 0.0783 mm d^{-1} (156 yr)$^{-1}$in FGOALS-g2 and 0.2180 mm d^{-1} (156 yr)$^{-1}$ in FGOALS-s2, while the dynamic component shows a significantly negative trend of −0.0521 (−0.0483) mm d^{-1} (156 yr)$^{-1}$ in FGOALS-g2 (FGOALS-s2) (Figs. 8e and f, Table 1). In other words, increasing moisture (thermodynamic mechanism) dominates over weakening circulation (dynamic mechanism) in changes of precipitation, which is consistent with results in previous studies (Chou and Lan, 2012; Chou et al., 2013; Huang et al., 2013; Held and Soden, 2006).

The contribution of each term to the water vapor budget is further addressed in Fig. 9. In the dry season, in both models, evaporation shows a significantly increasing trend, whereas the two moisture advection terms show a negative trend. The

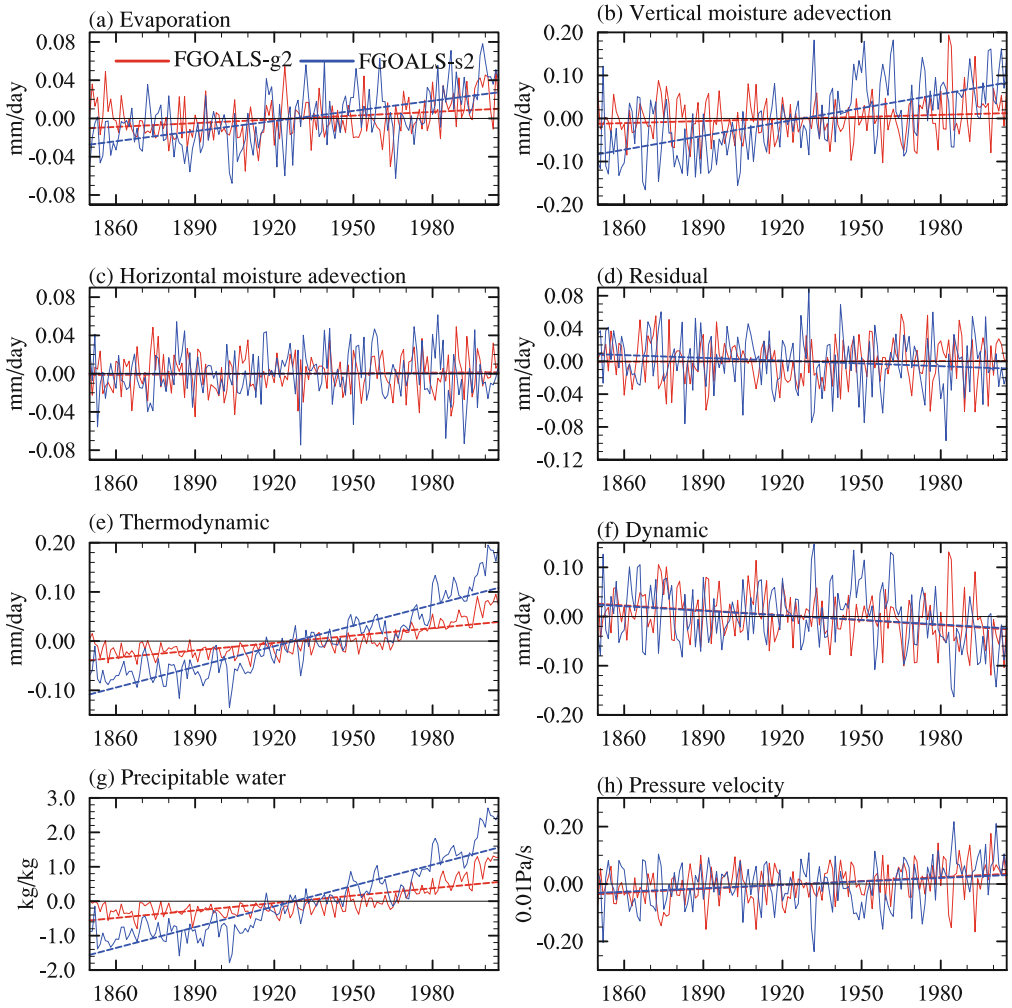

Fig. 8. Time series (1850–2005) of the different terms in the vertically integrated moisture budget equation for the wet season: (a) evaporation; (b) vertical moisture advection; (c) horizontal moisture advection; (d) residual term; (e) thermodynamic contributor; (f) dynamic contributor; (g) precipitable water vapor; (h) pressure velocity at 500 hPa. All time series are anomalies relative to the base period of 1850–2005. The units are mm d^{-1} in (a–f), kg kg^{-1} in (g), and 10^{-2} Pa s^{-1} in (h). The linear fits for all variables are also included. The red (blue) lines represent the historical run by FGOALS-g2 (FGOALS-s2). The left (right) axis correspond to the results of FGOALS-g2 (FGOALS-s2).

Table 1. Trends of globally averaged precipitation and moisture budget terms. Trends that are statistically significant at the 1% level are marked in bold font and with an asterisk. Units are mm d^{-1} (156 yr)$^{-1}$. Climatological norms are given in parentheses and units are mm d^{-1}.

	FGOALS-g2			FGOALS-s2		
	Wet Season	Dry Season	Annual Range	Wet Season	Dry Season	Annual Range
P	**0.0491*** (4.9058)	0.0017 (1.2840)	**0.0474*** (3.6219)	**0.2051*** (4.8711)	0.0115 (1.1203)	**0.1936*** (3.7508)
E	**0.0204*** (3.1583)	**0.0277*** (2.5550)	−0.0073 (0.6033)	**0.0550*** (3.6554)	**0.0485*** (2.7079)	0.0065 (0.9475)
$-\langle\omega\partial_p q\rangle$	0.0249 (1.9101)	−0.0020 (−1.0764)	0.0269 (2.9865)	**0.1675*** (1.8846)	**−0.0615*** (−1.0673)	**0.2290*** (2.9419)
$-\langle \boldsymbol{V}_h\cdot\nabla q\rangle$	0.0029 (0.0497)	**−0.0149*** (−0.2396)	**0.0177*** (0.2893)	0.0002 (0.0865)	**−0.0312*** (−0.2448)	**0.0314*** (0.3313)
δ	0.0010 (−0.2122)	−0.0091 (−0.0449)	0.0100 (−0.2572)	−0.0176 (−0.7455)	0.0557 (−0.2755)	−0.0733 (−0.470)
$-\langle\overline{\omega}\partial_p q'\rangle$	**0.0783***	**−0.0360***	**0.1142***	**0.2180***	**−0.1081***	**0.3261***
$-\langle\overline{\omega}'\partial_p\overline{q}\rangle$	**−0.0521***	**0.0332***	**−0.0853***	**−0.0483***	**0.0424***	**−0.0907***
$-\langle\omega'\partial_p q'\rangle$	0.0002	0.0004	−0.0002	−0.0020	**0.0044***	**−0.0064***
$\langle q\rangle$	**1.1232***	**0.8436***	—	**3.1359***	**2.2614***	—
ω_{500}	**0.0708***	**−0.0661***	—	**0.0623***	**−0.0613***	—

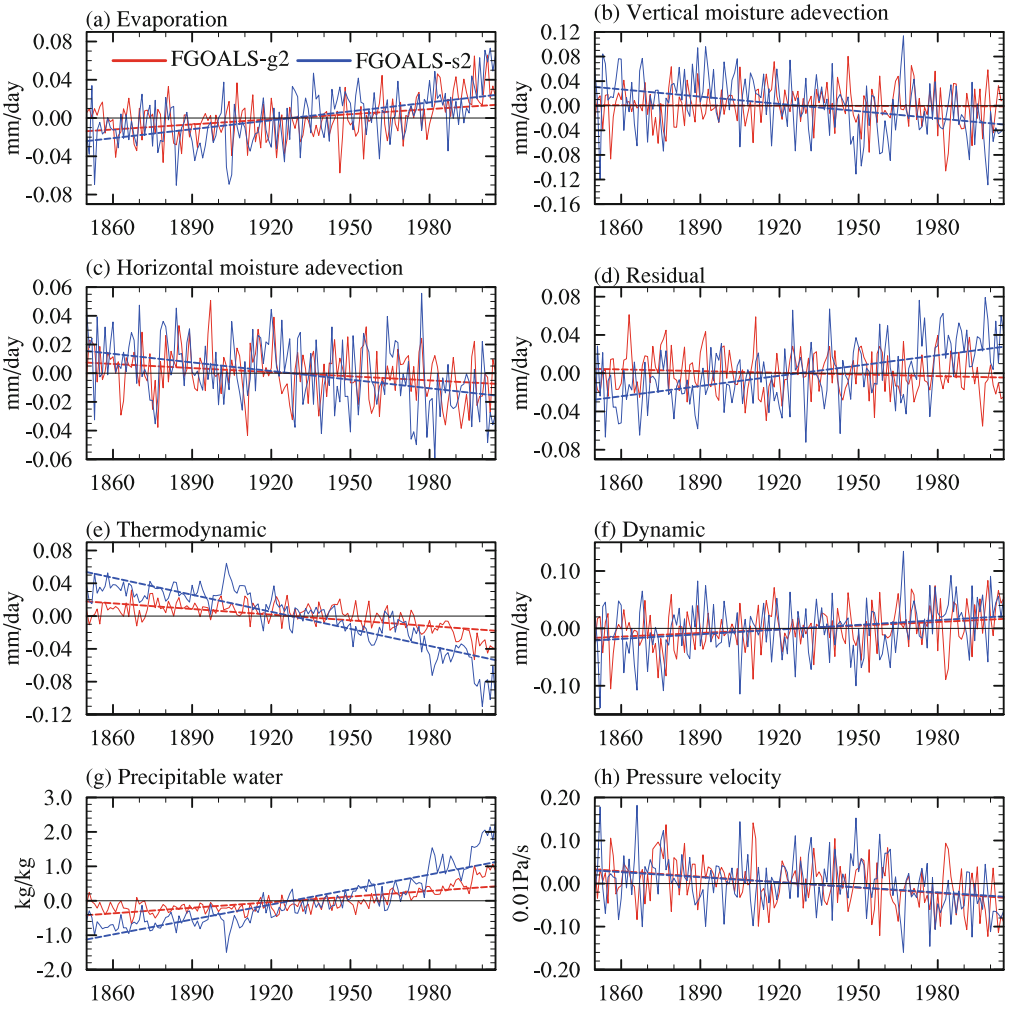

Fig. 9. As in Fig. 8 except for the dry season.

trend magnitude of horizontal moisture advection is comparable to that of the vertical moisture advection (Table 1). In the dry season, the vertical velocity is governed by descending motion. The vertical moisture advection contributes negatively to precipitation changes. In the two models, water vapor shows a weaker upward trend than that in the wet season,

while the weakening trend of descending motion is equivalent to that in the wet season. Accordingly, the change tendency of the thermodynamic (dynamic) component is downward (upward). The opposite trends between the evaporation (positive) and the moisture advection (negative) lead to a weak and insignificant change of precipitation in the dry season in the two models (Fig. 7d).

The change of the AR is dominated by the vertical moisture advection (Fig. 7e). A significant positive trend is seen in the vertical moisture advection term (Fig. 10). The effects of the horizontal moisture advection are stronger than those in the wet and dry seasons. In both models, the positive trends of vertical moisture advection and horizontal moisture advection combine to enhance the AR. The evaporation trends in the wet and dry seasons are nearly identical, and thus the contribution of evaporation to the enhanced AR is negligible. Therefore, the AR change is dominated by the vertical moisture advection. The trends of the thermodynamic and dynamic components in the wet season are opposite to those in the dry season, and so the trend amplitudes of both the thermodynamic and dynamic components for the AR are larger than their corresponding trends in the wet and dry seasons.

The above analyses demonstrate that the seasonal precipitation changes are dominated by both the vertical moisture advection and evaporation terms. The contribution of the thermodynamic component is the most important term.

4. Summary and discussion

4.1. *Summary*

The change of precipitation under global warming has been a useful metric for gauging model performance. In this study, the performances of two versions of the LASG/IAP's model FGOALS in reproducing the observed climatological mean state and changes of seasonal precipitation are evaluated. The mechanisms responsible for seasonal precipitation change are discussed. The analysis is carried out using the outputs of the 20th century (1850–2005) historical climate simulation experiments. The main conclusions are summarized below:

(1) Both versions of FGOALS reasonably reproduce the mean-state features of the timings of the wet and dry seasons, although a delayed occurrence of the wet and dry seasons is seen in the simulations in comparison to those of the observations.

(2) The climatology of precipitation in the wet and dry seasons and the AR are reproduced reasonably by both

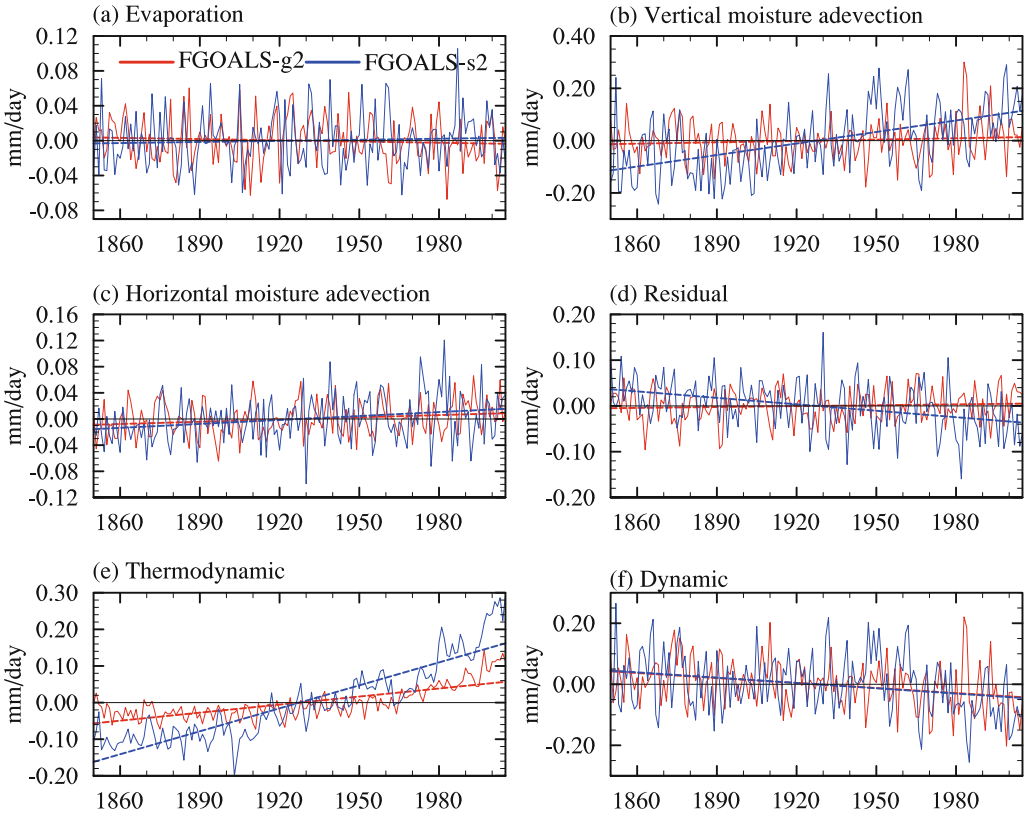

Fig. 10. Time series (1850–2005) of the different terms in the vertically integrated moisture budget equation for the annual range of precipitation: (a) evaporation; (b) vertical moisture advection; (c) horizontal moisture advection; (d) residual term; (e) thermodynamic contributor; (f) dynamic contributor. All time series are anomalies relative to the base period of 1850–2005. All units are mm d^{-1}. The linear fits for all variables are also included. The red (blue) lines represent the historical run by FGOALS-g2 (FGOALS-s2). The left (right) axis correspond to the results of FGOALS-g2 (FGOALS-s2).

FGOALS-g2 and FGOALS-s2. In the wet season, the PCC between the simulation and observation is 0.84 (0.83), the corresponding SDR is 1.10 (1.11) and the RMSD is 2.03 (2.11) for FGOALS-g2 (FGOALS-s2). In the dry season, the PCC, SDR and RMSD is 0.84 (0.78), 1.00 (1.16) and 0.86 (1.11) for FGOALS-g2 (FGOALS-s2), respectively. The PCC, SDR and RMSD values of the AR are 0.88, 1.11 and 1.78 (0.88, 1.09 and 1.79) for FGOALS-g2 (FGOALS-s2), respectively.

(3) The observed globally-averaged precipitation over 1979–2012 shows a significant increasing (decreasing) tendency at a rate of 0.2576 (-0.1699) mm d^{-1} (34 yr)$^{-1}$ in the wet (dry) season. The AR enhances at a rate of 0.4275 mm d^{-1} (34 yr)$^{-1}$. The models' responses are consistent with that in the observations, and both models reproduce a wetter wet season [0.0491 (0.2051) mm d^{-1} (156 yr)$^{-1}$ for FGOALS-g2 (FGOALS-s2)] and enhanced AR [0.0474 (0.1936) mm d^{-1} (156 yr)$^{-1}$ for FGOALS-g2 (FGOALS-s2)] over 1850–2005. Meanwhile, wetter wet seasons and an enhanced AR are seen in most regions of the world. The weakness of the simulation is that both models show a tendency of the dry season getting wetter, which is contrary to that in the observations. However, the observational data still contain uncertainties. Whether or not the difference results from model limitation or data quality deserves further study.

(4) Diagnoses on the outputs of the 20th century historical climate simulations of FGOALS-g2 and FGOALS-s2 show that the globally averaged seasonal precipitation changes are dominated by the changes of evaporation and vertical moisture advection. In the wet and dry seasons, evaporation contributes positively to precipitation change. For the AR changes, the contribution of evaporation is negligible. The vertical moisture advection term is the most important contribution to the changes of precipitation, wherein the thermodynamic component is dominant. The dynamic component tends to compensate for the effect of the thermodynamic component.

4.2. *Discussion*

Evaporation is an important process in the global water cycle (Held and Soden, 2006). Solar radiation hits the surface of water or land and causes water to change state from a liquid to a gas, leading water vapor to enter the atmosphere. The moisture in the atmosphere is linked to cloud formation and rainfall (Trenberth et al., 2003). Evaporation is one of the main water vapor sources of precipitation. One consequence of increased heating from the human-induced greenhouse effect is the increased evaporation of surface moisture (Yu and Weller, 2007). Thus, during 1850–2005, the response to global warming, regardless of whether for the wet season or dry season, the evaporation simulated by both versions of FGOALS exhibits a significantly increasing trend and then further facilitates the increase of precipitation. As the moisture supply for precipitation locally does not completely come directly from evaporation, some of it has to come from transport remotely and thus from convergence of low-level moisture elsewhere in the atmosphere (Trenberth et al., 2003). Meanwhile, the occurrence of the wet and dry seasons varies from grid to grid and year to year. So, as shown in our analysis, vertical moisture advection, which is closely connected with the low-level convergence of moisture, largely contributes to the change of global mean wet- and dry-season precipitation.

In the wet season, evaporation and vertical moisture advection combine to positively contribute to the formation of wetter wet seasons. In the dry season, the atmospheric circulation is dominated by lower-level divergence and vertical descending motion. Although evaporation in the dry season in both models shows increasing trends equivalent to that in the wet season, the cancellation effect of the vertical moisture advection (negative trend) results in an unobvious change of dry-season precipitation. As the increasing trends of evaporation are roughly equivalent in the wet and dry seasons, the enhancement of the AR mainly comes from the positive trend of vertical moisture advection.

The wet (dry) season is a period when floods (drought) occur frequently. The increased wet-season precipitation in the observations and simulations of the two versions of FGOALS may enhance the risk of floods, while the observed reduction of dry-season precipitation may enhance the risk of droughts.

Acknowledgements. This work was jointly supported by the National Natural Science Foundation of China (Grant Nos. 41125017 and 41330423). We thank the two anonymous reviewers for their valuable comments on the manuscript.

REFERENCES

Adler, R. F., and Coauthors, 2003: The Version 2 Global Precipitation Climatology Project (GPCP) monthly precipitation analysis (1979–present). *Journal of Hydrometeorology*, **4**, 1147–1167.

Andrews, T., P. M. Forster, O. Boucher, N. Bellouin, and A. Jones, 2010: Precipitation, radiative forcing and global temperature change. *Geophys. Res. Lett.*, **37**, L14701, doi: 10.1029/2010GL043991.

Allan, R. P., and B. J. Soden, 2008: Atmospheric warming and the amplification of precipitation extremes. *Science*, **321**, 1481–1484, doi: 10.1126/science.1160787.

Allan, R. P., B. J. Soden, V. O. John, W. Ingram, and P. Good, 2010: Current changes in tropical precipitation. *Environmental Research Letters*, **5**(2), 025205, doi: 10.1088/1748-9326/5/2/025205.

Bao, Q., and Coauthors, 2013: The Flexible Global Ocean-Atmosphere-Land System Model, Spectral Version 2: FGOALS-s2. *Adv. Atmos. Sci.*, **30**, 561–576, doi: 10.1007/s00376-012-2133-9.

Boer, G. J., 1993: Climate change and the regulation of the surface moisture and energy budgets. *Climate Dyn.*, **8**, 225–239.

Chadwick, R., I. Boutle, and G. Martin, 2013: Spatial patterns of precipitation change in CMIP5: Why the rich don't get richer in the tropics. *J. Climate*, **26**, 3803–3822.

Chen, X. L., T. J. Zhou, and Z. Guo, 2014: Climate sensitivities of two versions of FGOALS model to idealized radiative forcing. *Science China: Earth Sciences*, **57**, 1363–1373.

Chou, C., and J. Neelin, 2004: Mechanisms of global warming impacts on regional tropical precipitation. *J. Climate*, **17**, 2688–2701.

Chou, C., and C. Lan, 2012: Changes in the annual range of precipitation under global warming. *J. Climate*, **25**, 222–235.

Chou, C., J. Neelin, C. Chen, and J. Tu, 2009: Evaluating the "rich-get-richer" mechanism in tropical precipitation change under global warming. *J. Climate*, **22**, 1982–2005.

Chou, C., J. C. H. Chiang, C. W. Lan, C. H. Chung, Y. C. Liao, and C. J. Lee, 2013: Increase in the range between wet and dry season precipitation. *Nature Geoscience*, **6**, 263–267.

Flato, G., and Coauthors, 2013: Evaluation of climate models. *Climate Change 2013: The Physical Science Basis. Contribution of Working Group I to the Fifth Assessment Report of the Intergovernmental Panel on Climate Change*, Cambridge University Press, Cambridge, United Kingdom and New York, NY, USA, 741–866.

Held, I. M., and B. Soden, 2000: Water vapor feedback and global warming. *Annual Review Energy and the Environment*, **25**, 441–475.

Held, I. M., and B. J. Soden, 2006: Robust responses oh the hydrological cycle to global warming. *J. Climate*, **19**, 5686–5699.

Huang, P., S. P. Xie, K. Hu, G. Huang, and R. Huang, 2013: Patterns of the seasonal response of tropical rainfall to global warming. *Nature Geoscience*, **6**, 357–361.

Li, L., and Coauthors, 2013: The Flexible Global Ocean-Atmosphere-Land System Model, Grid-point Version 2: FGOALS-g2. *Adv. Atmos. Sci.*, **30**, 543–560, doi: 10.1007/s00376-012-2140-6.

Li, H., A. Dai, T. Zhou, and J. Lu, 2010: Responses of East Asian summer monsoon to historical SST and atmospheric forcing during 1950–2000. *Climate Dyn.*, **34**, 501–514.

Noake, K., D. Polson, G. Hegerl, and X. Zhang, 2012: Changes in seasonal land precipitation during the latter twentieth-century. *Geophys. Res. Letts.*, **39**, doi: 10.1029/2011GL050405.

Pal, I., B. T. Anderson, G. D. Salvucci, and D. J. Gianotti, 2013: Shifting seasonality and increasing frequency of precipitation in wet and dry seasons across the U.S. *Geophys. Res. Letts.*, **40**, 4030–4035, doi: 10.1002/grl.50760.

Polson, D., G. C. Hegerl, X. B. Zhang, and T. J. Osborn, 2013: Causes of robust seasonal land precipitation changes. *J. Climate*, **26**, 6679–6697, doi: 10.1175/JCLI-D-12-00474.1.

Pryor, S. C., and J. T. Schoof, 2008: Changes in the seasonality of precipitation over the contiguous USA. *J. Geophys. Res.*, **113**, D21108, doi: 10.1029/2008JD010251.

Qian, C., and T. Zhou, 2014: Multidecadal variability of North China aridity and its relationship to PDO during 1900–2010. *J. Climate*, **27**(3), 1210–1222.

Scheff, J., and D. Frierson, 2012: Twenty-first-century multimodel subtropical precipitation declines are mostly midlatitude shifts. *J. Climate*, **25**, 4330–4347.

Seager, R., N. Naik, and G. Vecchi, 2010: Thermodynamic and dynamic mechanisms for large-scale changes in the hydrological cycle in response to global warming. *J. Climate*, **23**, 4651–4668.

Taylor, K. E., R. J. Stouffer, and G. A. Meehl, 2012: An overview of CMIP5 and the experiment design. *Bull. Amer. Meteor. Soc*, **93**, 485–498.

Trenberth, K. E., A. Dai, R. M. Rasmussen, and D. B. Parsons, 2003: The changing character of precipitation. *Bull. Amer. Meteor. Soc.*, **84**, 1205–1217.

Trenberth, K. E., 2011: Changes in precipitation with climate change. *Climate Research*, **47**, 123–138.

Vecchi, G. A., and B. J. Soden, 2007: Global warming and the weakening of the tropical circulation. *J. Climate*, **20**, 4316–4340.

Vecchi, G. A., B. J. Soden, A. T. Wittenberg, I. M. Held, A. Leetmaa, and M. J. Harrison, 2006: Weakening of tropical Pacific atmospheric circulation due to anthropogenic forcing. *Nature*, **441**, 73–76.

Wang, B., and Q. H. Ding, 2006: Changes in global monsoon precipitation over the past 56 years. *Geophys. Res. Lett.*, **33**, L06711, doi: 10/1029/2005GL025347.

Wang, B, J. Liu, H. J. Kim, P. J. Webster, and S. Y. Yim, 2012: Recent change of the global monsoon precipitation (1979–2008). *Climate Dyn.*, **39**(5), 1123–1135.

Wang, B., J. Liu, H. J. Kim, P. J. Webster, S. Y. Yim, and B. Xiang, 2013: Northern Hemisphere summer monsoon intensified by mega-El Niño/southern oscillation and Atlantic multidecadal oscillation. *Proceedings of the National Academy of Sciences of the United States of America*, **110**(14), 5347–5352.

Wentz, F. J., L. Ricciardulli, K. Hilburn, and C. Mears, 2007: How much more rain will global warming bring? *Science*, **317**, 233–235.

William, K. L., H. T. Wu, and K. M. Kim, 2013: A canonical response of precipitation characteristics to global warming from CMIP5 models. *Geophys. Res. Letts.*, **40**, 3163–3169, doi: 10.1002/grl.50420.

Wu, B., and T. J. Zhou, 2013: Relationships between the East Asian-western North Pacific monsoon and ENSO simulated by FGOALS-s2. *Adv. Atmos. Sci.*, **30**(3), 713–725, doi: 10.1007/s00376-013-2103-6.

Xie, S. P., C. Deser, G. A. Vecchi, J. Ma, H. Teng, and A. T. Wittenberg, 2010: Global warming pattern formation: Sea surface temperature and rainfall. *J. Climate*, **23**, 966–986.

Yu, L. S., and R. A. Weller, 2007: Objectively analyzed air–sea heat fluxes for the global ice-free oceans (1981–2005). *Bull. Amer. Meteor. Soc.*, **88**, 527–539.

Zhang, X., F. W. Zwier, G. C. Hegerl, F. H. Lambert, N. P. Gillett, S. Solomon, P. A. Stott, and T. Nozawa, 2007: Detection of human influence on twentieth-century precipitation trends. *Nature*, **448**, 461–465.

Zhang, L. X., and T. J. Zhou, 2014: An assessment of improvements in global monsoon precipitation simulation in FGOALS-s2. *Adv. Atmos. Sci.*, **31**(1), 165–178, doi: 10.1007/s00376-013-2164-6.

Zhou, T. J., and R. C. Yu, 2006: Twentieth century surface air temperature over China and the globe simulated by coupled climate models. *J. Climate*, **19**(22), 5843–5858.

Zhou, T. J., Y. Q. Yu, H. L. Liu, W. Li, X. B. You, and G. Q. Zhou, 2007: Progress in the development and application of climate ocean models and Ocean-atmosphere coupled models in China. *Adv. Atmos. Sci.*, **24**(6), 1109–1120, 10.1007/s00376-007-1109-3.

Zhou, T. J., L. X. Zhang, and H. M. Li, 2008: Changes in global land monsoon area and total rainfall accumulation over the last half century. *Geophys. Res. Lett.*, **33**, doi: 10.1029/2008GL034881.

Zhou, T. J., D. Y. Gong, J. Li, and B. Li, 2009: Detecting and understanding the multi-decadal variability of the East Asian Summer Monsoon-Recent progress and state of affairs. *Meteorologische Zeitschrift*, **18**, 455–467.

Zhou, T. J., F. F. Song, and X. L. Chen, 2013a: Historical evolution of global and regional surface air temperature simu-

lated by FGOALS-s2 and FGOALS-g2: How reliable are the model results? *Adv. Atmos. Sci.*, **30**(3), 638–657, doi: 10.1007/s00376-013-2205-1.

Zhou, T., F. Song, R. Lin, X. Chen, and X. Chen, 2013b: The 2012 North China floods: Explaining an extreme rainfall event in the context of a long-term drying tendency [in "Explaining Extreme Events of 2012 from a Climate Perspective"]. *Bull. Amer. Meteor. Soc.*, **94**(9), S49–S51.

Zhou, T., Y. Yu, Y. Liu, and B. Wang, 2014: *Flexible Global Ocean–Atmosphere–Land System Model: A Modeling Tool for the Climate Change Research Community*. Springer, Heidelberg, 483 pp.

Zhou, Y. P., K. M. Xu, Y. C. Sud, and A. K. Betts, 2011: Recent trends of the tropical hydrological cycle inferred from Global Precipitation Climatology Project and International Satellite Cloud Climatology Project data. *J. Geophys. Res.*, **116**, D09101, doi: 10.1029/2010JD015197.